Wavelet Based Estimation of Local Kolmogorov Turbulence

George C. Papanicolaou
Knut Sølna

ABSTRACT We present a new approach for analyzing locally stationary processes with power law spectral densities. We divide the data into segments over which the process is essentially stationary and then use the wavelet scale spectrum to estimate the parameters of the power law, which are the scale factor and the exponent. These parameters vary from segment to segment, with part of the variation due to the nonstationarity of the data and part due to estimation errors that depend on the length of the segments. In the approach we introduce here, segmentation effects due to estimation errors are removed by filtering. We also estimate an effective local inertial range, that is, the set of scales over which the process can be modeled by a power law. We apply our estimation method to atmospheric temperature data that are expected to have Kolmogorov power law spectra. We find that there are significant fluctuations about the Kolmogorov law and analyze them in detail.

1 Introduction

Stochastic processes that are approximately stationary and have approximately power law spectral densities arise frequently in modeling atmospheric turbulence, financial data, geophysical data, etc. How can we estimate the variable power law behavior of the spectral densities from data? The analysis will depend on how we segment the data and on how we choose the range of scales, or frequencies, over which we look for a power law fit. In this paper we address these issues using fractional Brownian motion as the underlying stochastic model whose parameters are estimated locally by wavelet scale spectra. We then apply the theory to atmospheric turbulence data. This data was first analyzed in Washburn et al. [38] and subsequently in [22, 28, 33]. We provide here a general framework for estimating local power law processes with wavelets and a large part of the

AMS Subject classification: Primary 60G18; secondary 60M15.
Keywords and phrases: scale spectra, locally stationary time series, fractional Brownian motion, data segmentation, atmospheric turbulence

mathematical background needed for its justification. The motivation for the measurements and the analysis presented here is the propagation of a laser beam in the turbulent atmosphere. The beam will be affected by high frequency medium fluctuations that is caused by strong turbulence. The standard model used for such medium fluctuations is Fractional Brownian motion Washburn et al. [38]. We will model the medium in terms of *local* Fractional Brownian motion.

In Section 2 we introduce Fractional Brownian motion as a model for turbulence and discuss the wavelet based scale spectrum that can be used for spectral estimation of such processes.

In Section 3 we introduce the atmospheric data, and carry out a preliminary scale spectral analysis using the Haar-wavelet basis. This analysis suggests that nonstationary effects are indeed important for this data set. The range of scales over which the spectrum can be modeled as a power law, the inertial range, as it is called in turbulence theory, varies with spatial location and, in addition, the estimated power law parameters depend on location.

In Section 4 we discuss the method we use to estimate the power law parameters. First, in Section 4.2 we address the issue of choosing the range over which to fit the power law by regression. We do this by using the fractional Brownian motion as a model locally. Since the process is only locally stationary, power law parameters must be estimated based on relatively short spatial segments. In Section 4.3 we show how to remove the variability of the estimated power law parameters that is due to the finiteness of the segments. The filtering that we do here is used frequently in geostatistics [9, 31].

In Section 5 we return to the atmospheric data set and use the framework introduced in Section 4 for estimation of its spectrum. We segment the data into intervals over which they are approximately stationary. We must have a rough estimate of the size of the intervals of stationarity, which for the aerothermal data set we get from a variogram analysis of the wavelet coefficients. Another case where the intervals of stationarity are known approximately is analyzed in [2] using the local Fourier transform. We also show some simulations from the estimated model that assess the overall relevance of our analysis.

The main point of our analysis is that we are able to identify the local variations of the power law parameters, the Kolmogorov turbulence law, which arise from large scale atmospheric phenomena. The analysis should be applicable to other data sets, financial data for example, where departure from stationarity needs to be quantified.

Note that in order to deal with approximate stationarity and approximate power law spectra we need a good understanding of the estimation issues for stationary, power law processes, like fractional Brownian motion. Previous

work on the statistics of wavelet scale spectra of fractional Brownian motion can be found in [1, 13, 29, 36, 37, 39]. We provide in Section 6 a brief but complete analysis of these statistics that is based on a general formula for the covariance of the Haar wavelet coefficients (equation (6.2)). A central limit theorem for the estimators of the power law parameters also follows readily from the covariance formula, we show this in Section 7. When Fourier spectra are used the statistical analysis of global power law processes is given in [32] and an analysis of estimators for the exponent of the power law is given in [17, 21]. Taqqu and Teverovsky [35] present an empirical study that compares estimators for long-range dependence. We use wavelet scale spectra because they provide a time-scale decomposition of the data that is well suited to power law processes, whether they are stationary (have stationary increments) or not. A comparison of power law estimation based on wavelet scale spectra and on Fourier spectra, in the stationary case, is given in Abry el al. [1] and a common framework for estimation of long-range dependence discussed in [5].

2 Scale spectrum of Fractional Brownian motion

2.1 Fractional Brownian motion

We shall model 'pure' power law processes by fractional Brownian motion (fBm), $\{B_H(x); x \geq 0\}$, introduced by Mandelbrot and Van-Ness [24]. It is a Gaussian process with mean zero, stationary increments and covariance

$$E[B_H(x)B_H(y)] \;=\; \frac{\sigma^2}{2}(|x|^{2H} + |y|^{2H} - |x-y|^{2H}) \tag{2.1}$$

with $0 \leq H \leq 1$ and σ parameters. Its structure function is

$$E[(B_H(x) - B_H(x-\Delta x))^2] \;=\; \sigma^2|\Delta x|^{2H},$$

and it is conditioned to be zero at the origin: $B_H(0) = 0$. The so called Hurst exponent H determines the correlation of the increments. The covariance of future increments with past ones is

$$\begin{aligned}\rho_H(\Delta x) \;&=\; E[(B_H(x) - B_H(x-\Delta x)) \\ &\quad \times(B_H(x+\Delta x) - B_H(x))] \;=\; \sigma^2(2^{2H-1} - 1)|\Delta x|^{2H},\end{aligned}$$

which is independent of x. When $H > 1/2$ this quantity is positive so if the past increment is positive, then on average the future increment will be positive. Feder [11] calls this persistence. When $H < 1/2$ we have an antipersistent process with a positive increment in the past making a positive increment in the future less likely. Ordinary Brownian motion corresponds to $H = 1/2$. In this case future and past increments are independent. Of

special interest here is $H = 1/3$ which corresponds to the Kolmogorov scaling law [25].

Fractional Brownian motion has stationary increments but is not itself stationary. However, as shown in [1] for example, it is possible to assign a pseudo-spectrum to it by cutting off the low frequencies. Let

$$X = B_H * \psi$$

with star denoting convolution and ψ a function that integrates to zero so that its Fourier transform Ψ vanishes at zero frequency. The process X is stationary and its power spectrum is

$$P_X \quad \propto \quad \sigma^2 |f|^{-(2H+1)} |\Psi(f)|^2.$$

Since we usually observe power law processes through a filter that cuts off very low frequencies, we can associate with B_H the power law spectrum

$$\widetilde{P}_{B_H} \quad \propto \quad \sigma^2 |f|^{-(2H+1)} \ .$$

In the Kolmogorov case $H = 1/3$ the spectrum is $\sigma^2 |f|^{-5/3}$ over some range of frequencies, called the inertial range. Fractional Brownian motion is self-similar since $B_H(x)$ and $a^H B_H(x/a)$ have the same finite dimensional distributions for all a.

In Section 6 we discuss in detail estimation of fBm, or a pure power law process. In Section 4 below we generalize the estimation procedure to locally stationary power law processes and apply the scheme to the atmospheric data in Section 5.

2.2 Haar wavelets and scale spectrum

We want to carry out a spectral analysis of the process, given as a finite set of data, and to fit the estimated spectrum to a power law. For this purpose **scale** spectra, rather than Fourier spectra, will be used. Scale spectra are a natural and flexible tool for self-similar processes [1, 20]. The scale spectrum is defined in terms of the coefficients of the data in a wavelet basis. We will use the Haar wavelet basis although other bases could have been used as well [15]. In the application to the aerothermal data $H \approx 1/3$ but varying and this makes the Haar wavelets with relatively narrow support a natural choice. Haar wavelet based estimators are sometimes related to classical ones, as is in particular the Allan variance estimator for the slope of the log of the spectral density [30].

Let Y denote the process for which we want to compute the Haar wavelet coefficients. Denote the *approximation* coefficients at level zero by

$$X = (a_0(1), a_0(2), ..., a_0(2^M)).$$

These are defined by

$$a_0(n) = \int_{n-1}^{n} Y(x)dx \ .$$

Given this level zero representation, the data, we construct successively its wavelet coefficients with respect to the Haar basis as follows. Let

$$\begin{aligned} a_1(n) &= \frac{1}{\sqrt{2}}(a_0(2n) + a_0(2n-1)) \\ d_1(n) &= \frac{1}{\sqrt{2}}(a_0(2n) - a_0(2n-1)) \ , \quad \text{for} \quad n = 1, 2..., 2^{M-1} \end{aligned} \tag{2.2}$$

be the smoothed signal and its fluctuation, or detail, at the finest scale. Note that the *detail* vector d_1 contains every other successive difference of the data. This process of averaging and differencing can be continued by defining

$$\begin{aligned} a_2(n) &= \frac{1}{\sqrt{2}}(a_1(2n) + a_1(2n-1)) \\ d_2(n) &= \frac{1}{\sqrt{2}}(a_1(2n) - a_1(2n-1)) \ , \quad \text{for} \quad n = 1, 2..., 2^{M-2} \end{aligned}$$

and in general

$$\begin{aligned} a_j(n) &= \frac{1}{\sqrt{2}}(a_{j-1}(2n) + a_{j-1}(2n-1)) \\ d_j(n) &= \frac{1}{\sqrt{2}}(a_{j-1}(2n) - a_{j-1}(2n-1)) \ , \quad \text{for} \quad n = 1, 2..., 2^{M-j} \end{aligned}$$

for $j = 1, ..., M$. The data vector X can then be reconstructed from $a_M, d_M, d_{M-1}, ..., d_1$ since from equations (2.2) we have

$$\begin{aligned} a_0(2n) &= \frac{1}{\sqrt{2}}(a_1(n) + d_1(n)) \\ a_0(2n-1) &= \frac{1}{\sqrt{2}}(a_1(n) - d_1(n)) \ , \quad \text{for} \quad n = 1, 2..., 2^{M-1} \end{aligned}$$

and now a_1 can be replaced by sums and differences of a_2 and d_2, etc.

The detail coefficients at level j can alternatively be expressed as

$$d_j(n) = \frac{1}{\sqrt{2^j}} \int_{-\infty}^{\infty} \psi(x/2^j - n) Y(x) dx$$

with the mother wavelet defined by

$$\psi(x) = \begin{cases} -1 & \text{if} \quad -1 \le x < -1/2 \\ 1 & \text{if} \quad -1/2 \le x < 0 \\ 0 & \text{otherwise} \end{cases} \ .$$

The difference coefficients correspond to probing the process at different scales and locations, with n representing location and j scale. From the self-similarity of fractional Brownian motion it follows that for such a process $E[d_j(n)^2] \propto 2^{j(2H+1)}$.

The scale spectrum of X relative to the Haar wavelet basis is the sequence S_j defined by

$$S_j = \frac{1}{2^{M-j}} \sum_{n=1}^{2^{M-j}} (d_j(n))^2 \ , \quad j = 1, 2, ..., M. \tag{2.3}$$

For fractional Brownian motion the log of the scale spectrum is approximately *linear* in the scale j. As discussed in detail in Section 6 this can be used to estimate the parameters of the process by regression. It is easily verified from the definitions above that the l^2 norm of the data vector X can be written as

$$\sum_{n=1}^{2^M} (a_0(n))^2 = (a_M)^2 + \sum_{j=1}^{M} 2^{M-j} S_j \ ,$$

which is a way of expressing the orthogonality of the decomposition of X into a_M and the d_j, $j = 1, ..., M$.

The scale spectral point S_j is the mean square of the detail coefficients at scale j. The spectrum can therefore be interpreted as the energy of the signal in the different scales relative to the Haar wavelet basis. Consider data containing information only at the finest scale: $X = \{1, \ -1, \ 1, \ -1, \ \cdots\}$. Then only the $d_1(n)$ coefficients are non-zero. Hence, S_j roughly corresponds to the energy at $2^{(j-1)}$ times the finest scale.

Note that the spatial support of the integrals defining the wavelet coefficients at a certain scale is adapted to the particular scale. The short-scale difference coefficients, that provide high frequency information, are defined in terms of consecutive integrals of narrow support. A plot of these difference coefficients reveals information about how the high frequency content of the data changes with location.

3 The aerothermal data

3.1 Temperature and index of refraction fluctuations

Our objective is to estimate the spectrum of temperature data taken from the upper atmosphere. One motivation for our modeling and estimation is to be able to generate synthetic random media for the simulation of wave propagation, propagation of a laser beam, in a turbulent atmosphere. Before we analyze the aerothermal data we explain briefly how velocity,

temperature and index of refraction fluctuations are related to each other and how the Kolmogorov scaling theory enters in their description [25, 34].

The Kolomogorov theory is a phenomenological statistical description of the *velocity* field in the atmosphere. Based on a scaling argument, the mean-square velocity differences are described in a universal manner over a rather broad range of spatial scales, the inertial range. If we assume homogeneity, isotropy and incompressibility the result is that the structure function of the velocity has the form

$$E[(\mathbf{v_x}(\mathbf{x_0}+\mathbf{x})-\mathbf{v_x}(\mathbf{x_0}))^2] \;=\; C_{\mathbf{v}}^2|\mathbf{x}|^{2/3}. \tag{3.1}$$

Here $\mathbf{v_x}$ is the velocity in the direction of the displacement $\mathbf{x}$. The parameter $C_{\mathbf{v}}^2$ is the velocity structure constant, a measure of the amount of energy in the inertial range, which is typically confined between an inner scale l_0 and an outer scale L_0.

The connection to temperature is through the theory of convection-diffusion of a passive scalar. It turns out [25] that temperature fluctuations have also a structure function with Kolmogorov 2/3 scaling.

At optical frequencies the variations in the index of refraction δn are approximately

$$\delta n = -79P\frac{\delta T}{T^2}\times 10^{-6}$$

with P atmospheric pressure in millibars and T temperature in degrees Kelvin. Thus, in order to describe the spectrum of fluctuations in the refractive index we need only the spectrum of the fluctuations in the temperature. Wavelet scale spectra are used to analyze turbulence data in [19].

The above model for refractive index fluctuations is used extensively to model atmospheric wave propagation. Variations in the turbulent character of the medium are typically modeled through variations in $C_{\mathbf{v}}^2$ only and not in the exponent, which is fixed at 2/3.

3.2 Data analysis of aerothermal data

We will analyze temperature data obtained by the Air Force high-altitude laser propagation and turbulence data collection effort. For a detailed discussion of recording procedures and analysis see [28, 33, 38]. A strong effort was made to provide high quality data that could be used to characterize the turbulent atmosphere. The above references provide together a fairly detailed account for this unique data set.

We take the temperature data as our starting point and examine what analysis reveals about their structure. We are interested in particular in accounting properly for nonstationary effects. All calculations are carried out in MATLAB on a Silicon Graphics workstation.

PLACE FIGURE 1 HERE (FigPlotaero.ps)

In Figure 1 we show the temperature data, which has approximately 4.2×10^6 points. The spatial resolution is approximately 2cm. The data set has been recorded by a probe mounted on an aircraft and is, of course, quite noisy and it is part of our task to remove spurious noise effects in the estimation process.

PLACE FIGURE 2 HERE (FigPlotcoef.ps)

In Figure 2 we show a scale-space plot of the square of the Haar wavelet coefficients, corresponding to a plot of signal energy at different scales and locations. For short-scales or high frequencies a square wave that can be attributed to noise from the aircraft is clearly visible. For the long scales this component has been effectively suppressed by the lowpass filtering.

PLACE FIGURE 3 HERE (figmarg.ps)

PLACE FIGURE 4 HERE (figstatint.ps)

For fractional Brownian motion the wavelet coefficients will be normally distributed. In Figure 3 we show a histogram of the wavelet coefficients at scale 8, normalized by a local estimate of the variance. The dashed line corresponds to a Gaussian distribution. In the bottom plot we show the empirical variogram of these wavelet coefficients, normalized by their variance. The variogram is defined in (5.2) below. The dashed line is the theoretical variogram for fBm with Kolmogorov scaling, $H = 1/3$. In Figure 4 we show an estimate of the variogram function for $\log(d_j(n)^2)$; $7 \leq j \leq 9$. If the process had a pure power law spectrum over these scales we would see only a very small correlation. However, these quantities are correlated on the order of km, indicating that the data corresponds to a *local* power law.

Our main objective is now to examine whether the data can be modeled well by a 'power law' model over a subrange of scales. Recall that for such a process, the scale spectrum S_j is linear in a log-log plot, when the record is very long.

PLACE FIGURE 5 HERE (FigPlotScaleSpect.ps)

In Figure 5 we show log-log plots of scale spectra over nonoverlapping segments of the data, with each segment having length $655m$. The top plot corresponds to the first half of the data whereas the bottom plot corresponds to the second half. Each plot contains scale spectral points over 15 scales, $1 \leq j \leq 15$. This corresponds to length scales from $l_1 = .04m$ to $l_{15} = 655m$. We take as abscissa the spatial frequency K_j

$$K_j \;=\; \frac{\pi}{\Delta x} 2^{1-j} \text{ [rad/m]} \;=\; 100\pi 2^{-j} \text{ [rad/m]}. \tag{3.2}$$

Note that the scale spectra show a distinct departure from power law behavior for scales below one meter ($K = 6$). For larger scales, power law behavior may be considered in the range between $2.5m$ to $80m$ ($.08 \leq K \leq 2.5$) approximately, which corresponds to the detail coefficients d_7 to d_{12}. The departure from power law behavior for the shortest scales is partly due to the influence of measurement noise. The first half of the data is less en-

ergetic than the second half and has a higher signal to noise ratio. That the second half of the data is more energetic is also clearly seen in Figure 6. Here we segment the data into segments of length $655m$ and plot the mean square of the d_8 wavelets in each segment. It is the more energetic, strong turbulence, section that will affect propagation of a laser beam in the atmosphere. In the top plot of Figure 7 we show the data in this section. The laser beam will interact essentially only with the high frequency fluctuations in the medium. In Figure 7, bottom plot, we show the high-pass filtered temperature data, that is, the data restricted to scales 1 to 14 in a Daubechies ($db15$) wavelet basis. The high-pass filtering with a smooth wavelet mitigates the effects of the low order polynomial trens in the measured data that is seen in the top plot. A main motivation for our study is to estimate the turbulence parameter fluctuations that are important for laser beam propagation and we will focus on the strong turbulence section in between $50km$ and $85km$ in the estimation. Thus, we take the data in the bottom plot of Figure 7 as the starting point for our estimation of the turbulence parameters.

PLACE FIGURE 6 HERE (FigPlotlevel.ps)
PLACE FIGURE 7 HERE (FigPlotaeros.ps)

The parameter estimates, the estimated intercept and slope for the log scale spectra will depend on the particular segment of data used. We want to identify the part of this variability that is due to the nonstationarity of the process and minimize variability due to estimation errors. Before we continue with the scale spectral analysis we note the following.

- Noise bursts in the data enter only in some of the detail coefficients, as can be seen from Figure 2. The criterion for selecting of the inertial range, implemented in the next section, will automatically restrict the scale range.

- The temperature data are not a stationary time series and they do not have stationary increments. Computing scale spectra over *long* segments, in which the process cannot be taken as stationary, gives a quantity that is hard to interpret. Even though the average slope of the log scale spectra over several segments is close to $-5/3$, as the theory of turbulence predicts, there is a lot of variability. A **local** power law model of the kind discussed in Section 4 is likely to fit the data better than the idealized power law model, with stationary increments.

We will estimate the scale spectrum of the data when we model it as a local power law, using the method described in Section 4. To start the estimation we must have rough estimates for the intervals of stationarity and for the exponent of the power law. In view of Figures 3, 4 and 5 we choose these estimates to be

- $(\hat{\varepsilon})^{-1} = 2km$
- $H_0 = 1/3$ (Kolmogorov scaling) .

In the next section we develop a framework for estimation of local power law processes with varying inertial range and power law parameters. In Sections 5.1 and 5.2 we carry out the estimation. First we estimate the inertial range and then the power law parameters.

4 Estimation of local power law processes

4.1 Modeling and segmentation

The fractional Brownian motion described in Section 2 is an idealization of a process with power law spectrum. It has stationary increments and if the power law is truncated at low frequencies then it is itself stationary. In most physical or financial applications where power law behavior is expected locally, the power law parameters will vary so the process cannot be stationary in the large. The aerothermal data provide an example. We would like to estimate the power law parameters over segments that are short enough so that they can be taken as constant but long enough so that their statistical estimates are stable. How are we to decide what is a good segmentation of the data in this vague sense? This is a very difficult problem that is rarely addressed in theoretical or applied studies of spectral estimation. In Mallat et al. [23] a class of locally stationary processes is introduced and an algorithm for finding intervals of approximate stationarity is developed. This method is based on an exhaustive search for an optimal segmentation, in a suitable sense, into intervals of stationarity. It does not work so well when the intervals of stationarity are all of roughly the same size, and when dealing with turbulence data. Thus, here we follow a somewhat different approach where we can take advantage of prior information about intervals of stationarity, as is the case of the aerothermal data.

To fix ideas we will consider estimation of parameters for a multifractional Brownian motion (mBm), [8, 16, 29]. This is a generalization of fractional Brownian motion where the parameters vary with location. In the time domain the representation is

$$\begin{aligned} B_\varepsilon(x) &= \frac{\sigma_\varepsilon(x)}{\Gamma(H_\varepsilon(x)+1/2)} \int_{-\infty}^{0} [(x-s)^{H_\varepsilon(x)-1/2} - (-s)^{H_\varepsilon(x)-1/2}] dW(s) \\ &\quad + \int_0^x (x-s)^{H_\varepsilon(x)-1/2} dW(s) \end{aligned} \tag{4.1}$$

with W the standard Brownian motion and

$$H_\varepsilon(x) = H(\varepsilon x) \tag{4.2}$$

$$\sigma_\varepsilon(x) = \sigma(\varepsilon x) \tag{4.3}$$

where $H(\cdot)$ & $\sigma(\cdot)$ can be deterministic or random. For example, they can be stationary stochastic processes with smooth paths and decaying correlation functions, independent of the Brownian path $W(\cdot)$. When H and σ are constants then (4.1) is a time domain representation of the usual fractional Brownian motion. In the application to aerothermal data the Hurst exponent vary smoothly around 1/3 corresponding to Kolmogorov turbulence. We assume here that the process $H \in \mathcal{C}^1$ and takes values in $(0, 1)$ as in [7]. Note that mBm also has been generalized to more irregular functions H, see [3, 6].

The parameter ε^{-1} is a measure of the interval of stationarity in the sense that, as in [16]

$$E[(B_\varepsilon(x) - B_\varepsilon(x - \Delta x))^2] \;\approx\; \sigma_\varepsilon^2(x)|\Delta x|^{2H_\varepsilon(x)}$$

for $\varepsilon\Delta x$ small. This means that for scales that are small compared to the interval of stationarity, the processes $B_\varepsilon(x)$ behaves locally like a fractional Brownian motion with parameters frozen at x.

In Section 4.3 we will describe a method that removes dependence of the estimated parameters on a prior estimate of the interval of stationarity. The basic idea is that we know roughly what $1/\varepsilon$ should be and how the estimation errors behave if the underlying process is fractional Brownian motion, given the segment size. We then filter out these estimation errors and get estimates that do not depend sensitively on the prior choice of the size of the interval of stationarity.

Another modification that is necessary in the nonstationary case is the identification of the inertial range over each interval of approximate stationarity. The error in the power law fit to the scale spectra, over a segment of data, depends on the scale range that is used. How do we select a range of scales for which the error in the fit is acceptable? In the next section we introduce a criterion for selecting the range based on comparison with an ideal fractional Brownian motion.

4.2 Estimation of the inertial range

The power law behavior that we want to identify in the data is necessarily restricted to a finite set of scales, the inertial range, in each segment of stationarity.

Let 2^M denote the length of the data vector over the segment under consideration. For an ideal fractional Brownian motion with Hurst exponent H let $S_i,\ i = 1, \ldots, M$ be its wavelet scale spectrum. Then, for each subrange $\{i_1, \cdots, i_2\}$ the measure of misfit

$$r(i_1, i_2) \;=\; \sum_{i=i_1}^{i_2} [\log_2(S_i) - \log_2(\hat{S}_i)]^2, \tag{4.4}$$

with $\hat{S}_i$ the power law estimated by weighted least squares, is a random variable whose law can be computed analytically in principle or numerically. It depends weakly on H so we fix it to equal some rough estimate $H = H_0$. For the aerothermal data of Section 3 we take $H_0 = 1/3$, the Kolmogorov exponent. Let $R(i_1, i_2)$ be the 90th percentile of the distribution of $r(i_1, i_2)$ with the value of the Hurst parameter equal to H_0. The scale range is now chosen as the *largest* range $\{i_1, \cdots, i_2\}$ for which $\tilde{r}(i_1, i_2) < R(i_1, i_2)$. Here $\tilde{r}(i_1, i_2)$ is the value of the error (4.4) obtained from the actual data.

In order to obtain stable power law parameter estimates in the regression we need a minimum number of scale range points. In the application to the aerothermal data introduced in Section 3 we choose to model in terms of a power law only over segments for which there are 5 or more points in the estimated scale range.

4.3 Segmentation independent power law estimation

Given a fixed segmentation of the data into approximate intervals of stationarity that is based on some prior information, we first calculate the inertial range as described in the previous section and then do the power law fit. The power law parameters are obtained by weighted linear regression of the log scale spectrum, see Section 6.4. The estimated power law parameters depend on the segmentation. We will now describe a method with which this dependence can be removed.

The idea is to do a filtering of the parameter estimates in order to remove the variability that is segmentation dependent. From the theory of the power law estimators for fractional Brownian motion we know that the slope estimator has the form

$$\hat{p}^i \;=\; p^i + w^i \tag{4.5}$$

where p^i is the slope for the i'th segment and w^i the fluctuation due to the finiteness of the segment. We cannot take large segments, that reduce this error, because we are limited by the nonstationarity. The errors w^i are essentially uncorrelated over different segments and we have to construct a filter that will predict p^i from the estimates $\hat{p}^i$ by removing the noise w^i, to the extent possible. We assume that p^i is itself a stationary stochastic process, independent of the Brownian motion that generates the fractional Brownian motion. The p^i are the intrinsic variation of the power in the locally stationary fractional Brownian motion. The correlation length of the p^i must be longer than the segments used in estimating them in order to have approximate stationarity relative to the segmentation.

It can be shown using the results from Section 6 that w^i is close to being a white process. This is important because it allows us to estimate the autocovariance of p^i from the estimates $\hat{p}^i$, using the variogram, for example. Given estimates of the autocovariance of p^i and the variance of w^i

we can design a minimum mean square error predictor or smoothing filter for p^i.

The minimum variance unbiased filter for prediction of the parameter processes is as follows. We describe it in the context of the slope parameter, but the filtering of the log intercept is completely analogous. Let $\hat{\mathbf{P}} = (\hat{p}_i)$ be the vector of estimates, $\mathbf{P} = (p_i)$ the realization of the slope process and $\bar{\mathbf{P}} = (\bar{p})$ the constant mean. Then the filter Γ is a matrix that transforms $\hat{\mathbf{P}}$ into $\Gamma\hat{\mathbf{P}}$ in such a way that

$$E[||\Gamma\hat{\mathbf{P}} - \mathbf{P}||^2]$$

is minimized over all matrices Γ that also preserve the mean $\bar{\mathbf{P}}$ of $\mathbf{P}$, that is $\Gamma\bar{\mathbf{P}} = \bar{\mathbf{P}}$. Let C_p be the covariance matrix of $\mathbf{P}$. Then it easily follows that

$$\Gamma \;=\; (C_p + C_w)^{-1}[C_p + \mathbf{u}^T \otimes \bar{\mathbf{P}}]$$

where the vector $\mathbf{u} = (u_i)$ is given by

$$u_i \;=\; \frac{\bar{\mathbf{P}}_i - \bar{\mathbf{P}}^T(C_p + C_w)^{-1}C_{p,i}}{\bar{\mathbf{P}}^T(C_p + C_w)^{-1}\bar{\mathbf{P}}}$$

and C_w is the diagonal covariance matrix of the estimation errors w^i. Here $C_{p,i}$ is the $i-$th column of the matrix C_p and the superscript T stands for transpose. The slope and log intercept processes are filtered separately. Filtering of this kind is discussed in [9, 31] for example.

Since the effect of the sample noise w^i in (4.5) is largely removed by the filtering procedure, the estimates of the parameter processes will be essentially independent of the prior choice of segmentation.

5 Application to aerothermal data

5.1 Estimation of inertial range

We estimate the set of scales where the process can be modeled as a 'power law'. Figure 5 shows that it varies with location. That is, the set of scales where the scale spectrum is approximately linear is location dependent. There are two main reasons for this. First, the scale range where the physical process has power law spectrum varies and depends on the local intensity of the turbulence. Second, the set of scales that are affected by measurement noise varies depending also on the intensity of the turbulence.

We use the scheme described in Section 4.2 to estimate the inertial range. First, we choose a segmentation that is short relative to the prior estimate of the interval of stationarity. We choose segments of length 2^{15} points. Then we apply the algorithm of Section 4.2. For all scale ranges we measure the difference between the scale spectrum computed from the data and the

fitted power law and choose the estimated scale range as the largest one for which this measure is within the 90th percentile of the corresponding measure for a realization of fractional Brownian motion.

The estimated 'effective inertial ranges' are shown in Figure 8, top plot, by the vertical solid lines. For each segment there is one vertical line showing the scales included in the corresponding effective inertial range. The segments consist of 2^{15} points and the maximum scale considered is 14.

PLACE FIGURE 8 HERE (FigPlotinertial.ps)

In Figure 8, bottom plot, we show the average of the spectra. The averaging is carried out *before* the log transformation. Note the excellent match with the Kolmogorov scaling law shown by the solid line!

5.2 Estimation of power law parameters

In the previous Section we estimated the inertial range for the scale spectrum, relative to a fixed segmentation. We will now estimate the power law parameters over this set of constrained scales. We use the method described in Section 4.3 for this purpose. Our main objective is to capture the intrinsic variation in the parameters. If we choose a coarse segmentation the variability of the estimates will be small. However, the estimated power law based on the scale spectrum may in this case be an average of power law parameters that vary within the section. Therefore we must choose a segmentation that is not much larger than the interval of stationarity. The estimates should be independent of segmentation. That is, if we shorten the segments this should not lead to an increase in the variability of the estimated parameters.

To show that this is achieved by filtering we choose the following segmentations

$$160m\ (2^{13}\text{ points}),\ 327m\ (2^{14}),\ 655m, (2^{15}).$$

There are 256, 128, 64 nonoverlapping segments, respectively, in each case.

We use the linear least squares regression

$$\log S_j^i \approx c^i + p^i \log_2(\frac{2^j}{50}) \tag{5.1}$$

for each segment i, with j the scale in suitable units. In Section 6 we analyze the regression of (5.1). The results of the estimation are shown in Figure 9.

PLACE FIGURE 9 HERE (FigPlotPar.ps)

We see from the figure that the estimated slopes, $\hat{p}$, vary considerably over the data set. They also depend on the segmentation, with the finer ones having larger fluctuations (solid lines). The difference between the parameter estimates is mainly due to a white noise estimation residual. This leads us to the second step of the estimation. In this step we carry

out a filtering procedure in order to remove the sampling variability that is segmentation dependent. We use the filtering described in Section 4.3. From the first step we obtained the estimates (in the case of the slopes)

$$\hat{p}^i \;=\; p^i + w^i \;.$$

The filter computes the minimum variance unbiased predictor of p^i given $\hat{p}^i$.

To construct the minimum variance unbiased filter we need the some additional estimates that we get from the process $\hat{p}^i$. We assume that the correlation of the sampled slope process is approximately exponential. We show below that an exponential function approximates the correlations of the sampled slope process well. We need, therefore, its correlation length l_p and its variance σ_p^2

$$E[(p_i - \bar{p})(p_j - \bar{p})] \;=\; \sigma_p^2 \exp(-L|i-j|/l_p)$$

with L the length of the segments. Note that this model is intrinsic to the process and does not depend on the segmentation. As discussed above we shall model the sample noise process $\{w_i\}$ as white and we only need its level σ_w^2. We estimate the parameters σ_p^2, l_p and σ_w^2 using the empirical variogram.

For a time series $\mathbf{X} = (X_i)$ of size N the empirical variogram with lag j is defined by

$$V(j) = \frac{1}{2(N-j)} \sum_{k=1}^{N-j} (X_{k+j} - X_k)^2 \tag{5.2}$$

with dependence on the length of the data vector N not shown. The mean of the empirical variogram for the slope process $\hat{\mathbf{P}}$ is

$$E[V(j)] \;=\; \sigma_p^2(1 - \exp(-L|j|/l_p)) + \sigma_w^2$$

and from this we obtain the parameter estimates by fitting to the empirical variogram. In particular, σ_w^2 is given by the vertical intercept since the process $\{w_i\}$ is white.

We estimated also the log-intercepts for the three segmentations. The estimated parameters are as follows for respectively the slope and the log-intercept:

- **For the slope**: Vertical intercept $\sigma_w^2 = 0.07$, horizontal asymptote level $\sigma_w^2 + \sigma_p^2 = 0.2$, and correlation length $800m$ (five segment lengths).

- **For the log intercept**: Vertical intercept $\tilde{\sigma}_w^2 = 0.5$, horizontal asymptote level $\tilde{\sigma}_w^2 + \sigma_c^2 = 3.5$, and correlation length $800m$ (five segment lengths).

The magnitue of the white noise part given above, σ_w, coincides with the one that follows from the asymptotic theory presented in Section 6. Note the relatively small value of $\tilde{\sigma}_w$. These estimates are obtained using the finest segmentation, $160m$, and only the data in the last half section, the high turbulence section. The estimates were based on slope process obtained by regression as above, but for the *fixed* set of scales 7 to 12. In this case the magnitude of the estimation error does not depend on the segment. We show the correlation structure in Figure 10. The solid line is the fitted model. There are two parts to it, the sampling noise part (the intercept) and the exponential part corresponding to intrinsic variation in the parameters.

PLACE FIGURE 10 HERE (FigPlotvariop.ps)

Using the estimated model parameters we carry out the filtering to get a better estimate for the slope and log intercept processes. In Figure 11 we show these filtered slope processes. Note that after the filtering all three segmentations give essentially the same result, as expected. Moreover, observe the strong intrinsic variation in the slope parameter. Figure 12 shows the corresponding filtered intercept processes.

PLACE FIGURE 11 HERE (FigPlotFiltp.ps)

PLACE FIGURE 12 HERE (FigPlotFilti.ps)

We next simulate synthetic temperature profiles using the parameters estimated above. Recall that we only aim to model the process on the scales corresponding to the turbulent inertial range. We therefore *scale* filter both the aerotherman data of Figure 1 and the synthetic temperature profile so that only the coefficients in the Haar wavelet basis corresponding to the inertial range contribute. Figure 13 shows the scale filtered processes. The similarity between the processes is striking. Next, we assess the accuracy of the parameter estimates by applying the estimation procedure to simulated data. We find that the standard deviations for the local slope and log-intercept estimates are .15 and .3 respectively.

PLACE FIGURE 13 HERE (FigPlotScfilt.ps)

5.3 Summary and conclusions

We have generalized the estimation of fractional Brownian motion to a procedure for estimation of a local power law process. For such processes the power law itself (the exponent or slope) and the multiplicative constant (log intercept of the scale spectrum) are not constants but vary slowly. We estimate the slope and log intercept of the scale spectrum by appropriately segmenting the data and then removing segmentation effects by a filtering procedure. The slope and log intercepts themselves are modeled as stochastic processes. The estimation of the power law includes the identification of a location dependent inertial range, that is, the scale range where the process can be modeled as a power law.

We applied the estimation procedure to an important set of aerothermal

data. We found that the *average* of the estimated slope process is close to the value predicted by the Kolmogorov scaling theory. To get a faithful representation of the heterogeneity in the data it is however important to incorporate the local fluctuations around this value.

Realizations from the estimated power law model can be used to define synthetic media for wave propagation codes. This is the application that motivated our investigation. A complete study of the effects of the heterogeneity in local power law model on wave propagation has yet to be carried out.

An important aspect of the model that we use is separation of scales in the variation of the estimated parameters (slope and log intercept) from the scale at which we sample the process.

Thus, we have shown how to generalize a procedure for estimation of *pure* fractional Brownian motion to estimation of a *local* power law. In the next two sections we analyze in detail estimation of *pure* fractional Brownian motion based on the Haar scale spectrum and obtained excellent agreement between theory and simulation.

6 On estimation of fractional Brownian motion

6.1 Statistics of wavelet coefficients for fBm

The scale spectrum is based on the wavelet coefficients. We now consider the statistics of the Haar wavelet coefficients for fBm. Next we will analyze the scale spectrum and power law parameter estimates based on these statistics. We assume that the data given to us is the wavelet approximation coefficients at level zero. That is, we assume that

$$a_0(n) = \int_{n-1}^{n} B_H(x)dx \ . \tag{6.1}$$

The wavelet coefficients are therefore normally distributed random variables with

$$\begin{aligned} E[d_j(n)] &= 0 \\ Var[d_j(n)] &= \sigma^2 \frac{(1-2^{-2H})}{(2H+2)(2H+1)} 2^{j(2H+1)} \\ Cor[d_{j_1}(n_1)d_{j_2}(n_2)] &= \frac{|D/\sqrt{l}|^{2H+2}}{8(2^{2H}-1)} \{\delta^2_{l/D}\delta^2_{1/D}|x|^{2H+2}\}|_{x=1} \ . \end{aligned} \tag{6.2}$$

Here

$$l = 2^{j_2-j_1}, \quad j_1 \le j_2 \tag{6.3}$$

is the relative scale,

$$D \;=\; |(2n_2-1)l-(2n_1-1)| \tag{6.4}$$

is the relative location and

$$\delta_d^2 f(x) = f(x+d) - 2f(x) + f(x-d) \tag{6.5}$$

is the second order symmetric difference. These results are derived using (2.1) and self-similarity of fBm. Note that the expression for the correlation of the wavelet coefficients takes on a universal form depending only on the relative displacement in space and scale. The derivation of the precision of the power law estimators in Section 6.3 is based on (6.2), which was only known in special cases before [13, 36].

Consider the correlation of wavelet-coefficients, when

$$\frac{D}{l} \;=\; |2^{j_2}(2n_2-1) - 2^{j_1}(2n_1-1)|2^{-j_2} \;\to\; \infty$$

then

$$\frac{\delta^2_{l/D}}{(l/D)^2}\frac{\delta^2_{1/D}}{(1/D)^2}$$

is a forth order central difference operator and its expansion gives the asymptotic result

$$Cor[d^{n_1}_{j_1}, d^{n_2}_{j_2}] \;=\; \frac{(H+1)(2H+1)H(2H-1)}{2(2^{2H}-1)}\left[\left(\frac{\sqrt{l}}{D}\right)^{2-2H} + \mathcal{O}\left(\frac{\sqrt{l}}{D}\right)^{4-2H}\right].$$

If the scales j_1 and j_2 are given, then for $n_2 \to \infty$ and n_1 fixed we have that $\frac{\sqrt{l}}{D} \approx \frac{1}{2n_2\sqrt{l}}$, whereas for $n_1 \to \infty$ and n_2 fixed we have $\frac{\sqrt{l}}{D} \approx \frac{\sqrt{l}}{2n_1}$. The correlation within a single scale is in particular

$$\begin{aligned} &Cor[d^{n_1}_{j}, d^{n_2}_{j}] \qquad\qquad (6.6)\\ &= \frac{(H+1)(2H+1)H(2H-1)}{2(2^{2H}-1)}\left[\left(\frac{1}{2|n_2-n_1|}\right)^{2-2H} + \mathcal{O}\left(\frac{1}{|n_2-n_1|}\right)^{4-2H}\right]. \end{aligned}$$

For general wavelets the following asymptotic result is presented in [13, 36]

$$\begin{aligned} E[d^{n_1}_{j_1} d^{n_2}_{j_2}] \;&\sim\; \mathcal{O}(|2^{j_2}n_2 - 2^{j_1}n_1|^{2(H-R)}) \\ &\text{for}\;\; |2^{j_2}n_2 - 2^{j_1}n_1| \;\to\; \infty \end{aligned}$$

with R being the number of vanishing moments for the wavelet ($R=1$ for Haar wavelets).

6.2 Statistics of the scale spectrum

Using the above results for the wavelet coefficients we get a characterization of the statistics of the scale spectral points. The mean is

$$\begin{aligned} E[S_j] &= E[d_j(n)^2] = \sigma^2 h(H) 2^{j(2H+1)} \\ &\propto \int_{-\infty}^{\infty} \sigma^2 |f|^{-(2H+1)} \frac{\sin^4(\pi 2^{j-1} f)}{(\pi 2^{j-1} f)^2} 2^j df \end{aligned} \tag{6.7}$$

where

$$h(H) = \frac{(1 - 2^{-2H})}{(2H+2)(2H+1)} \ . \tag{6.8}$$

The normalized variance is

$$\frac{Var[S_j]}{E[S_j]^2} = 2\frac{\sum_{n,m}(C^j_{nm})^2}{N_j^2 E[S_j]^2} = \frac{1}{N_j}\left\{ \frac{4}{N_j} \sum_{k=0}^{N_j-1} (N_j - k)\rho_H^2(k) - 2 \right\} \tag{6.9}$$

with $N_j = 2^{M-j}$, the number of detail coefficients at level j and 2^M the total length of the data. Note that here and in the sequel we suppress the dependence on M. The matrix $C^j = (C^j_{nm})$ in (6.9) is the covariance matrix of the wavelet coefficients at scale j, determined by (6.2), and $\rho_H(k)$ is the corresponding correlation coefficient, which depends only on $k = |n_1 - n_2|$ and H. Denote

$$g(H) = \lim_{N_j \to \infty} \left\{ \frac{4}{N_j} \sum_{k=0}^{N_j-1} (N_j - k)\rho_H^2(k) - 2 \right\} \tag{6.10}$$

then

$$\frac{Var[S_j]}{E[S_j]^2} \sim \frac{g(H)}{N_j} \text{ for } N_j \to \infty \ . \tag{6.11}$$

The function $g(H)$ is computed numerically and is shown in Figure 14. It depends only weakly on the value of H, especially when $H \leq 1/2$ which is the case of interest to us. The asymptotic behavior (6.11) holds only when the correlation $\rho_H^2(k)$ decays to zero in an integrable way. This means that the Hurst exponent must be restricted to $H < 3/4$. In the Kolmogorov case $H = 1/3$, the correlation ρ_H decays like $k^{-4/3}$.

PLACE FIGURE 14 HERE (figgfunc.ps)

Similarly, if $H < 3/4$, the normalized covariance can be expressed, for *fixed* scale separation, as

$$R_{j_1 j_2} \equiv \frac{Cov[S_{j_1}, S_{j_2}]}{E[S_{j_1}]E[S_{j_2}]} = 2\frac{\sum_{n,m}(C^{j_1,j_2}_{nm})^2}{N_{j_1} N_{j_2} E[S_{j_1}]E[S_{j_2}]} \tag{6.12}$$

with C^{j_1,j_2} being the cross covariance between the wavelet coefficients at scale j_1 and j_2, determined by (6.2). The scale spectral points S_j are not uncorrelated for different j, as is sometimes assumed. For the power law parameter estimation we note that for fixed j_1 and j_2

$$R_{j_1 j_2} \equiv \frac{Cov[S_{j_1}, S_{j_2}]}{E[S_{j_1}]E[S_{j_2}]} \sim \frac{1}{\sqrt{N_{j_1} N_{j_2}}} \tag{6.13}$$

as N_{j_1} and N_{j_2} go to infinity. These results can be derived using (6.2).

6.3 Fluctuation theory for the scale spectra

In the least squares fit of the power law we will need the statistical properties of the logarithm of the scale spectra. We summarize the relevant facts in this section, with the details given in Section 7.

In the large N_j limit, the *distribution* of the scale spectral points is normal

$$\begin{aligned} S_j &= \bar{S}_j(1 + \frac{v_j}{\sqrt{N_j}}) \\ v_j &\sim \mathcal{N}(0, g(H)) \text{ for } N_j \to \infty \end{aligned}$$

with $\bar{S}_j \equiv E[S_j] = \sigma^2 h(H) 2^{j(2H+1)}$ and where h and g are defined by (6.8) and (6.10), respectively, and $\mathcal{N}(\mu, s^2)$ is the normal distribution with mean μ and variance s^2. The derivation of these results requires that $H \leq 1/2$. The covariance of the fluctuations is

$$Cov[\frac{v_j}{\sqrt{N_j}}, \frac{v_i}{\sqrt{N_i}}] = R_{ji} \tag{6.14}$$

with R_{ji} given by (6.13).

The fluctuations in S_j are small and in Section 7 we show that this leads to the asymptotic estimate

$$\begin{aligned} \log_2(S_j) &= \log_2(\bar{S}_j) + \frac{\bar{v}_j}{\sqrt{N_j}\ln(2)} \\ \bar{v}_j &\sim \mathcal{N}(0, g(H)) \text{ for } N_j \to \infty \ . \end{aligned} \tag{6.15}$$

In addition to showing that v_j is asymptotically normal, we also show in Section 7 that for any $j_1 < j_2$ fixed the random variables $v_j,\ j_1 \leq j \leq j_2$, are asymptotically jointly normal, as $N_j \to \infty$.

6.4 Estimators for the power law

Write (6.15) as

$$\begin{aligned} \log_2(S_j) &= \log_2(\sigma^2 h(H)) + j(2H+1) + \frac{\bar{v}_j}{\sqrt{N_j}\ln(2)} \\ &= c + jp + \frac{\bar{v}_j}{\sqrt{N_j}\ln(2)} \quad j_1 \leq j \leq j_2 \end{aligned} \tag{6.16}$$

with the slope p and log intercept c to be estimated from data, and $\bar{v}_j/\sqrt{N_j}$ a fluctuation term that is characterized in the large N_j limit by the central limit theorem, as discussed in the previous section. In view of the above we can use generalized least squares to estimate $\mathbf{b} = [c, p]^T$ as

$$\hat{\mathbf{b}} = (X^T R^{-1} X)^{-1} X^T R^{-1} \mathbf{Y} \tag{6.17}$$

with $\mathbf{Y} = [\log_2(S_{j_1}), \cdots, \log_2(S_{j_2})]^T$, and where $j_1, \cdots, j_2$ are the scales in the range under consideration, the inertial range. The dependence on j_1, j_2 and M has been suppressed. For a discussion of generalized least squares see [18]. The design matrix X is defined as

$$X = \begin{bmatrix} 1 & j_1 \\ 1 & j_1 + 1 \\ \vdots & \vdots \\ 1 & j_2 \end{bmatrix} .$$

The matrix R is the normalized covariance matrix of the spectral points defined in (6.12). This matrix depends on the value of H. However this dependence is weak so we can use some rough estimate of H that is usually available, like $H = 1/3$ for the aerothermal data of Section 5. In view of (6.16) we find that the estimates of $\mathbf{b}$ have means

$$\begin{aligned} E[\hat{c}] &= \log_2(\sigma^2 h(H)) \\ E[\hat{p}] &= 2H + 1 \end{aligned} \tag{6.18}$$

and covariance

$$C_{\mathbf{b}} = (X^T R^{-1} X \ln(2)^2)^{-1} = \frac{\ln(2)^{-2}}{[\sum\sum R_{ij}^{-1} \sum\sum R_{ij}^{-1}\ i\ j - (\sum\sum R_{ij}^{-1})^2]}$$

$$\times \begin{bmatrix} \sum\sum R_{ij}^{-1} & -\sum\sum R_{ij}^{-1}\ i \\ -\sum\sum R_{ij}^{-1}\ i & \sum\sum R_{ij}^{-1} i\ j \end{bmatrix} \sim \frac{1}{N_{j_1}} \text{ for } N_j \to \infty \tag{6.19}$$

From the above we arrive at the sought after parameter estimates

$$\hat{H} = (\hat{p} - 1)/2 \tag{6.20}$$

$$\widehat{\log_2(\sigma^2)} = \hat{c} - \log_2(h(\hat{H})) \ . \tag{6.21}$$

We next analyze the precision of these estimators. We find that the estimates $\hat{H}$ and $\widehat{\log_2(\sigma^2)}$ are normally distributed with variances

$$Var[\hat{H}] = C_{\mathbf{b}}(2,2)/4 \tag{6.22}$$

$$Var[\widehat{\log_2(\sigma^2)}] \sim C_{\mathbf{b}}(1,1) - 2C_{\mathbf{b}}(1,2)\ \log_2(h(H))' + C_{\mathbf{b}}(2,2)\ [\log_2(h(H))']^2$$

for N_{j_1} large with $C_{\mathbf{b}}$ defined in (6.19) and h in (6.8). The variance of the estimators is of order $1/N_{j_1}$.

Long-memory processes can also be modeled via state space models. Maximum likelihood estimators (MLE) for such models are analyzed in [10, 14].

6.5 Illustration of precision

The above result on the distribution of the estimators may be illustrated with numerical simulation. We generate synthetic realizations of fractional Brownian motion with known parameters. Then we use the above algorithm to estimate these parameters and compare the precision of the estimates with the predicted precision. Actually, we do not simulate fractional Brownian motion but rather the observed sequence (6.1), the approximation coefficients at level zero. The synthetic realizations are generated by a simulation algorithm similar to the one discussed in [27].

In Figure 15 we compare the asymptotic law of the estimators with simulations. It is clear that the theoretical normal distribution predicts accurately the distribution of the estimators.

PLACE FIGURE 15 HERE (figdistr.ps)

We show how the variance of the slope estimate $\hat{p}$ depends on the number of scales in the linear fit and the total number of data-points in Figure 16. The dotted and solid lines correspond to using respectively scales $1, 2, 3$ and scales $1, \cdots, 5$ and Hurst parameter $H = 1/3$. The crosses give the Cramer-Rao lower bound [1, 40]: $1/(2^{M+2}\ln^2(2))$ for the case that the wavelet coefficients are uncorrelated. The figure shows that only a few scales are needed for the variance of the slope estimator to be close to the bound.

PLACE FIGURE 16 HERE (figprec.ps)

Note that our objective is estimation of H when $H \approx 1/3$ and that our asymptotic result is valid only when $H < 1/2$. Several authors [26] have observed that slope estimators degrade when H become large ($H \approx 1$). This is because in that case the wavelet coefficients exhibit long-range correlations. Estimation for long-range processes corresponding to $H > 1/2$ is discussed in [4].

In the application of the estimation of the power law parameters to the aerothermal data in Section 5, which we model by a local fractional Brownian motion, we have to account for spurious noise effects. This noise affects the small scales mostly. We can make the power law parameter estimates more robust by letting the weight matrix R in (6.17) depend on an additive noise parameter which must be adjusted appropriately from rough prior data analysis. This is done in Section 5.2 without a detailed discussion.

7 Central limit theorem for scale spectra

In this section we derive a central limit theorem for the scale spectral points, S_j, and also the log transformed spectral points $\log_2(S_j)$, where

$$S_j = \frac{1}{N_j}\sum_{n=1}^{N_j}(d_j(n))^2$$

with $(d_j(n))_{n=1}^{N_j}$ the Haar difference coefficients of fractional Brownian motion at scale j with $H \leq 1/2$. The total number of data points is 2^M and $N_j = 2^{M-j}$. We will consider the limit $N_j \to \infty$. This means that M is large and that j is not too close to M, that is, the central limit theorem will not be valid for the large-scale spectral points S_j with $j \approx M$. We will use the following version of the Berry-Esseen theorem [12].

Let the y_i be independent random variables such that

$$E[y_i] = 0,\ E[y_i^2] = \sigma_i^2,\ E[|y_i^3|] = \rho_i,$$

define

$$s_n^2 = \sum_{i=1}^{n} \sigma_i^2,\ r_n = \sum_{i=1}^{n} \rho_i$$

and let F_n be the distribution of the normalized sum $\sum_{i=1}^{n} y_i/s_n$.
Then for all x and n

$$|F_n(x) - \mathsf{N}(x)| \ \leq \ 6\frac{r_n}{s_n^3} \tag{7.1}$$

where N stands for the mean zero, unit variance normal distribution.

7.1 Central limit theorem for S_j

To use this theorem we will first transform the sum of squares of wavelet coefficients to a sum of independent random variables. Denote the vector of wavelet coefficients at scale j by $d^j = [d_j(1), \cdots, d_j(N_j)]^T$ and the covariance matrix associated with d^j by C^j. Then d^j has the same law as

$$(C^j)^{1/2}[\eta_1, \cdots, \eta_{N_j}]^T$$

and in law

$$S_j \ = \ \frac{\bar{S}_j}{N_j}\sum_{i=1}^{N_j} \lambda_i^j \eta_i^2 \ = \ \bar{S}_j \left(1 + \frac{1}{\sqrt{N_j}}[\frac{1}{\sqrt{N_j}}\sum_{i=1}^{N_j} \lambda_i^j(\eta_i^2 - 1)]\right) \tag{7.2}$$

where η_i are independent zero mean and unit variance normal random variables, $\bar{S}_j = E[S_j]$ and λ_i^j are the eigenvalues of $C^j/\bar{S}_j$, the correlation matrix of d^j.

Let

$$Y_j \ = \ \frac{1}{\sqrt{N_j}}\sum_{i=1}^{N_j} y_i^j$$

with $y_i^j = \lambda_i^j(\eta_i^2 - 1)$. Note that the y_i^j are independent random variables such that

$$E[y_i^j] = 0,\ E[(y_i^j)^2] = 2(\lambda_i^j)^2,\quad E[|(y_i^j)^3|] \leq 28(\lambda_i^j)^3\ .$$

According to (7.1) we need only show that

$$J_j \ \equiv\ \frac{\sum_{i=1}^{N_j}(\lambda_i^j)^3}{[\sum_{i=1}^{N_j}(\lambda_i^j)^2]^{3/2}} \tag{7.3}$$

is small for N_j large.

Using (6.9) we find

$$\begin{aligned}\sum_{i=1}^{N_j}(\lambda_i^j)^2 \ &=\ \sum_{n,m}(C_{nm}^j/\bar{S}_j)^2 \qquad (7.4)\\ &=\ N_j^2 Var[S_j]/(2\bar{S}_j^2)\ \sim\ N_j\ g(H)/2 \text{ for } N_j\ \to\infty.\end{aligned}$$

Below we show that

$$\lambda_i^j\ \leq\ K \tag{7.5}$$

for some constant $K \geq 1$ independent of N_j. Hence

$$\sum_{i=1}^{N_j}(\lambda_i^j)^3\ \leq\ N_j K^3\ . \tag{7.6}$$

From (7.4) and (7.6) we find

$$J_j\ \approx\ \frac{(2K^2/g(H))^{3/2}}{\sqrt{N_j}}$$

and goes to zero as $N_j \to \infty$. From the Berry-Esseen theorem we conclude that the distribution of

$$Y_j/\sqrt{g(H)}\ =\ \frac{\sum_{i=1}^{N_j}\lambda_i^j(\eta_i^2-1)]}{\sqrt{g(H)N_j}}$$

tends to the standard normal distribution as N_j becomes large.

Thus

$$S_j\ \sim\ \bar{S}_j(1+\epsilon_j\sqrt{\frac{g(H)}{N_j}}) \text{ for } N_j \to \infty$$

in law, with ϵ_j a standard normal random variable.

Let us now show (7.5). The diagonal entries of the correlation matrix are all equal to one. By the Gersgorin disc theorem, $|\lambda_i^j - 1| \leq \sum_{n\neq i}|C_{in}|/C_{11}$. But the sum remains finite as $N_j \to \infty$ because we have assumed that $H \leq 1/2$ and so we can use (6.6). Rewriting the inequality with λ_i^j on the left side we get (7.5).

7.2 Central limit theorem for $\log_2(S_j)$

We consider next a central limit theorem for $\log_2[S_j]$. As in (7.2) we write the scale spectrum in terms of centered random variables Y_j

$$S_j \;=\; \bar{S}_j(1+\frac{Y_j}{\sqrt{N_j}}) \; .$$

Taking logs and expanding in a Taylor expansion with remainder we get

$$\log_2(S_j) \;=\; \log_2(\bar{S}_j) + \frac{Y_j}{\sqrt{N_j}\ln 2} - \frac{Y_j^2}{2\xi(Y_j)^2 N_j \ln 2}$$

with

$$\xi(Y_j) \in \begin{cases} (1, 1+Y_j/\sqrt{N_j}) & \text{when } Y_j \geq 0, \\ (1+Y_j/\sqrt{N_j}, 1) & \text{when } Y_j < 0. \end{cases}$$

We showed above that the central limit theorem holds for Y_j. We show below that $Y_j^2/(2\xi(Y_j)^2)$ is $\mathcal{O}(1)$ as $N_j \to \infty$. We therefore, have a central limit theorem for $\log_2(S_j)$ as well.

By the Cauchy-Schwarz inequality

$$\mathcal{J}_j \;\equiv\; E\left[|\frac{Y_j^2}{\xi(Y_j)^2}|\right] \;\leq\; \sqrt{E[\xi(Y_j)^{-4}]E[Y_j^4]} \; .$$

We show that $\mathcal{J}_j = \mathcal{O}(1)$ as $N_j \to \infty$. Consider first $E[Y_j^4]$. Using (7.5) we find

$$\begin{aligned} E[Y_j^4] \;&=\; E[(\frac{\sum_{i=1}^{N_j}\lambda_i^j(\eta_i^2-1)]}{\sqrt{N_j}})^4] \\ &\leq\; K^4(N_j E[(\eta_i^2-1)^4] + N_j(N_j-1)6E^2[(\eta_i^2-1)^2])/N_j^2 \;=\; c_1 + c_2/N_j \end{aligned}$$

with c_i constants. Next consider

$$\begin{aligned} I_j \;&\equiv\; E[\xi(Y_j)^{-4}] \;\leq\; E[\xi(Y_j)^{-4} I_{(Y_j\leq 0)}] + 1 \\ &\leq\; E[(1+Y_j/\sqrt{N_j})^{-4} I_{(Y_j\leq 0)}] + 1 \end{aligned}$$

with I_A the indicator function of the set A. In order to bound I_j we replace $1+Y_j/\sqrt{N_j}$ by Z_j such that w.p.1 $Z_j \leq (1+Y_j/\sqrt{N_j})$.

Note that

$$1+Y_j/\sqrt{N_j} \;=\; \frac{\sum_{i=1}^{N_j}\lambda_i^j\eta_i^2}{N_j}$$

and that $\sum_{i=1}^{N_j}\lambda_i^j = N_j$, which is the trace of the correlation matrix for d^j. Let q be the number of eigenvalues that exceed $1/2$. In view of (7.5) we find

$$q \;\geq\; \tilde{N}_j \;=\; N_j(2K-1)^{-1} \;\equiv\; N_j\tilde{K} \; .$$

Thus, we can define Z_j as

$$Z_j \;=\; \frac{1}{2}\frac{\sum_{i=1}^{\tilde{N}_j}\tilde{\eta}_i^2}{N_j} \;=\; \frac{\tilde{K}}{2}\frac{\sum_{i=1}^{\tilde{N}_j}\tilde{\eta}_i^2}{\tilde{N}_j}.$$

Hence

$$I_j \;\leq\; E[Z_j^{-4}I_{(Y_j\leq 0)}]+1 \;\leq\; (2/\tilde{K})^4\tilde{N}_j^4E[\tilde{Z}^{-4}]+1$$

with

$$\tilde{Z}_j \;=\; \sum_{i=1}^{\tilde{N}_j}\eta_i^2$$

in law. The random variable $\tilde{Z}_j$ has law given by the Gamma density

$$\gamma_{(\alpha,\nu)}(x) \;=\; \frac{(\alpha)^\nu}{\Gamma(\nu)}\,x^{\nu-1}\,\exp(-\alpha x)$$

with parameters $\alpha = 1/2$ and $\nu = \tilde{N}_j/2$. It follows that for $\tilde{N}_j \geq 10$

$$E[\tilde{Z}^{-4}] \;=\; \frac{(\alpha)^\nu\Gamma(\nu-4)}{(\alpha)^{\nu-4}\Gamma(\nu)} \;=\; \frac{1}{(\tilde{N}_j-2)(\tilde{N}_j-4)(\tilde{N}_j-6)(\tilde{N}_j-8)}\,.$$

Hence, $I_j \leq K''$ and

$$\mathcal{J}_j \;\leq\; \sqrt{K''(c_1/N_j+c_2)} \;\leq\; \bar{K}$$

for $N_j \geq 10/\tilde{K}$.

From the above we conclude that

$$\log_2(S_j) \;\sim\; \log_2(\bar{S}_j)+\epsilon_j\sqrt{\frac{g(H)}{N_j\ln(2)}} \text{ for } N_j\to\infty$$

in law, with ϵ_j a standard normal random variable.

7.3 Joint density of spectral points

We show that the spectral points are asymptotically, as $N_j \to \infty$, *jointly* normal. A generalization of the argument presented in Section 7.2 shows that this is the case also for the log spectral points. From this follows that the central limit theorem holds also for the power law parameter estimates. Consider the distribution of $Y = a_1S_{j_1} + a_2S_{j_2}$ with $a_1 \neq 0$, $a_2 \neq 0$ and $j_1 < j_2$ fixed parameters. The central limit theorem for this quantity can be

shown essentially as in Section 7.1. Let d^{j_1} and d^{j_2} be the vectors of wavelet coefficients at the two scales. Define

$$d \;=\; \left[\begin{array}{c} d^{j_1} \\ d^{j_2} \end{array} \right]$$

and $\tilde{d} = \Sigma d$ with Σ a diagonal matrix whose first N_{j_1} elements equal $\sqrt{a_1}$ and last N_{j_2} elements equal $\sqrt{a_2 2^{j_1 - j_2}}$. Then

$$Y = \tilde{d}^T \tilde{d}/N_{j_1} \; .$$

By a transformation to independent variables and an application of the Berry-Esseen theorem we find, as in (7.3), that we need to show

$$J \;\equiv\; \frac{\sum_{i=1}^{N_{j_1}+N_{j_2}} (\lambda_i)^3}{[\sum_{i=1}^{N_{j_1}+N_{j_2}} (\lambda_i)^2]^{3/2}} \tag{7.7}$$

is small for N_{j_1} large. Here λ_i are the eigenvalues of $Cov(\tilde{d}) = \Sigma C \Sigma$ with C the covariance matrix of d. Note first that from (6.9) it follows

$$\sum_{i=1}^{N_{j_1}+N_{j_2}} \lambda_i^2 \;\geq\; (a_1)^2 \sum_{n,m} (C_{nm}^{j_1})^2 \;\sim\; (a_1)^2 N_{j_1} (\bar{S}_{j_1})^2 g(H)/2 \text{ for } N_j \to \infty \; .$$

Hence, the result follows if we can bound λ_i uniformly with a bound independent of N_{j_1}. We find, using (6.2) and the Gersgorin disc theorem, that for some constant L and $1 \leq j \leq N_{j_1}$

$$|\lambda_j - a_1 \bar{S}_{j_1}| \;\leq\; L \bar{S}_{j_1}$$

since the rows of C are absolutely and uniformly summable with a bound that is independent of N_{j_1}. Hence $\lambda_i \leq \tilde{L} \bar{S}_{j_1}$ for some constant $\tilde{L}$. A similar argument holds for $N_{j_1} < j \leq N_{j_1} + N_{j_2}$. Therefore, J defined in (7.7) is small for N_j large and the central limit theorem for Y follows.

Acknowledgment. We thank D. Washburn for providing the data.
This work was partially supported by AFOSR grant F49620-98-1-0211, by ONR grant N00014-96-1-0719 and by NSF grant DMS-9709320 at Stanford University and by NSF Grant DMS-0093992 at University of California at Irvine.

References

[1] Abry, P., Goncalves, P., and Flandrin, P., (1995), "Wavelets, Spectrum Analysis and $1/f$ Processes," in *Wavelets and Statistics,* eds. A. Antoniadis and G. Oppenheim, Springer Lecture Notes in Statistics 103, Springer Verlag, pp. 15-29.

[2] Asch, M., Kohler, W., Papanicolaou, G., Postel, M., and White, B., (1991), "Frequency Content of Randomly Scattered Signals," in *Siam Review,* 33, pp. 519-626.

[3] Ayache, A., and Levy Vehel, J., (2000), "The Generalized Multifractional Brownian Motion," in *Statistical Inference for Stochastic Processes*, 3, pp. 85-99.

[4] Bardet, J. M., Lang, G., Moulines, E., and Soulier, P., (2000), "Wavelet Estimator of Long-Range Dependent Processes", in *Statistical Inference for Stochastic Processes*, 3 , pp. 101-111.

[5] Bardet, J. M., Moulines, E., and Soulier, P., (1998), "Recent advances on the semi-parametric estimation of long-range dependence coefficient", ESAIM Proceedings, 5, pp. 29-41.

[6] Benassi, A., Bertrand, P., Cohen, C., and Istas J., (2000), "Identification of the Hurst Index of a Step Fractional Brownian Motion," in *Statistical Inference for Stochastic Processes*, 3 , pp. 101-111.

[7] Benassi, A., Cohen, C., and Istas J., (1998), "Identifying the multifractional function of a Gaussian process", *Stat. Prob. Lett.*, 39, pp. 338-345.

[8] Benassi, A., Jaffard, S., and Roux, D., (1997), "Gaussian processes and pseudodifferential elliptic operators", *Rev. Mat. Iberoamericana*, 13, (1), pp. 19-81.

[9] Cressie, N., (1993), *Statistics for Spatial Data,* Wiley New York.

[10] Dahlhaus, R., (1989), "Efficient Parameter Estimation for Self-similar Processes," in *Annals of Statistics,* 17, pp. 1749-1766.

[11] Feder, J., (1988), *Fractals,* Plenum Press, New York.

[12] Feller, W., (1970), *An Introduction to Probability Theory and its Applications,* Vol II, Wiley.

[13] Flandrin, P., (1992), "Wavelet Analysis and Synthesis of Fractional Brownian Motion," in *IEEE Transactions on Information Theory,* 38, pp. 910-917.

[14] Fox, R., and Taqqu, M., (1986), "Large-sample Properties of Parameter Estimates for Strongly Dependent Stationary Gaussian Time Series," in *Annals of Statistics*, 14, pp. 517-532.

[15] Goncalves, P., and Abry, P., (1996), "Multiple Window Wavelet Transform and Local Scaling Exponent Estimation," in Research Report, INRIA.

[16] Goncalves, P., and Flandrin, P., (1992), "Scaling Exponents Estimation from Time-scale Energy Distributions," in *IEEE International Conference on Acoustics, Speech and Signal Processing,* ICASSP-92, San Francisco, pp. V.157-V.160.

[17] Hall, P., Koul, H.L., and Turlach, B.A., (1997), "Note on Convergence Rates of Semiparametric Estimators of Dependence Index," in *Annals of Statistics,* 25, pp. 1725-1739.

[18] Hardle, E., (1991), *Smoothing Techniques,* Springer Verlag.

[19] Hudgins, L., Friehe, C.A., and Mayer, M.E., (1993), "Wavelet Transforms and Atmospheric Turbulence," in *Physical Review Letters,* 71, pp. 3279-3282.

[20] Kaiser, G., (1994), *A Friendly Guide to Wavelets,* Birkhäser.

[21] Kent, J.T., and Wood, A.T.A., (1997), "Estimating the Fractal Dimension of a Locally Self-similar Gaussian Process by Using Increments," in *Journal of the Royal Statistical Society B,* 3, pp. 679-700.

[22] Kruger, V., Rino, C., Papanicolaou, G., and Sølna, K., (1998), "Analysis of Aerothermal Data," VISTA Inc. Report, 100 View St., Mountain View CA 94041.

[23] Mallat, S., G. Papanicolaou and Zhang, Z., (1998), "Adaptive Covariance Estimation of Locally Stationary Processes," in *Annales of Statistics,* 26, pp. 1-47.

[24] Mandelbrot, B.B., and Van Ness, J., (1968), "Fractional Brownian Motion, Fractional Noises and Applications," in *SIAM Review,* 10, pp. 422-437.

[25] Monin, A.S. and Yaglom, A.M., (1971), *Statistical Fluid Mechanics: Mechanics of Turbulence.* Vol. 1. The MIT Press.

[26] Ninness, B., (1998), "Estimation of 1/f Noise," in *IEEE Transactions on Information Theory,* 44, pp. 32-46.

[27] Omre, H., Sølna, K., and Tjelmeland, H., (1993), "Simulations of Random Functions on Large Lattices," in *Geostatistics,* Eds. A. Soares, pp. 179-199, Kluwer Academic Publishers.

[28] Papanicolaou, G., Sølna, K., and Washburn, D., (1998), "Segmentation Independent Estimates of Turbulence Parameters," in *SPIE AeroSense Meeting,* Orlando Florida.

[29] Peltier, R.F., and Levy-Vehel, J., (1995), "Multifractional Brownian Motion: Definition and Preliminary Results," Research Report, INRIA, 1995.

[30] Percival, D.B., and Guttorp, P., (1994), "Long-memory Processes, the Allan Variance and Wavelets, in *Wavelets in geophysics,* Eds. E. Foufoula-Georgiou and P. Kumar, pp. 325-344, Academic Press.

[31] Ripley, B., *Spatial Statistics,* Wiley, New York, 1981.

[32] Robinson, P.M., (1995), "Log-periodogram Regression of Time Series with Long Range Dependence," in *Annals of Statistics,* 23, pp. 1048-1072.

[33] Rossi, L., Kaiser, G., Washburn, D., (1998), "Recovery of Kolmogorov Statistics in Thermal Mixing in the Troposphere: The Hazards of Real Data," SPIE Meeting Orlando Florida.

[34] Strohbehn, J.W., (1978), *Laser Beam Propagation in the Atmosphere,* Springer Verlag, 1978.

[35] Taqqu, M.S., and Teverovsky, V., (1995), "Estimators for Long-range Dependence: An Empirical Study," in *Fractals,* 3, pp. 785-798.

[36] Tewfik, A.H., and Kim, M., (1992), "Correlation Structure of the Discrete Wavelet Coefficients of Fractional Brownian Motions," in *IEEE Transaction on Information Theory,* 38, pp. 904-909.

[37] Wang, Y, Cavanaugh, J.E. and Song, C., (1997), "Self-similarity Index Estimation via Wavelets for Locally Self-similar Processes," preprint, Department of Statistics, University of Missouri, Columbia, MO.

[38] Washburn, D., Banton, D.W., Brennan, T.T., Brown, W.P., Butts, R.R., Coy, S.C., Dueck, R.H., Koenig, K.W., Masson, B.S., Peterson, P.H., Praus, R.W., Tyler,G.A., Venet, B.P., and Weaver, L.D., (1996), "Airborne Laser Extended Atmospheric Characterization Experiment (ABLE ACE).", Technical report, Phillips Laboratory, Kirtland Air Force Base NM 87117-5776.

[39] Wornell, G.W., (1996), *Signal Processing with Fractals, a Wavelet Based Approach,* Prentice Hall.

[40] Wornell, G.W., and Oppenheim, A.V., (1992), "Estimation of Fractal Signals from Noisy Measurements Using Wavelets," in *IEEE Transactions on Signal Processing,* 40, pp. 611-623.

George C. Papanicolaou, Department of Mathematics, Stanford University, Stanford, CA 94305, U.S.A., e-mail: papanico@math.stanford.edu

Knut Sølna, Department of Mathematics, University of California at Irvine, Irvine, California 92697, U.S.A., e-mail: ksolna@math.uci.edu

FIGURE 1 (FigPlotaero.ps)

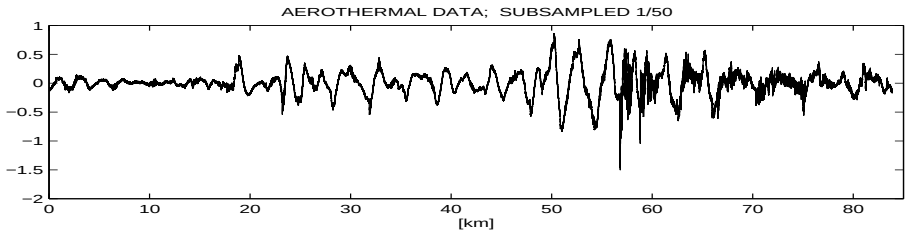

FIGURE 1. The raw temperature data. The spatial resolution of the data is approximately 2cm.

FIGURE 2 (FigPlotcoef.ps)

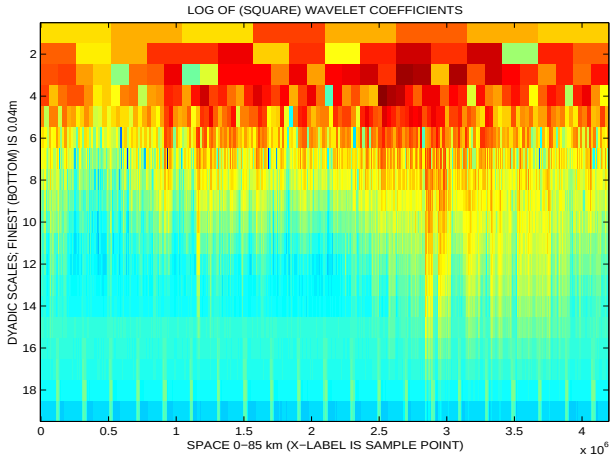

FIGURE 2. The square Haar wavelet coefficients for different scales and locations which corresponds to a scale-space energy distribution. Measurement noise gives rise to the square wave that is seen for the shortest scales.

FIGURE 3 (figmarg.ps)

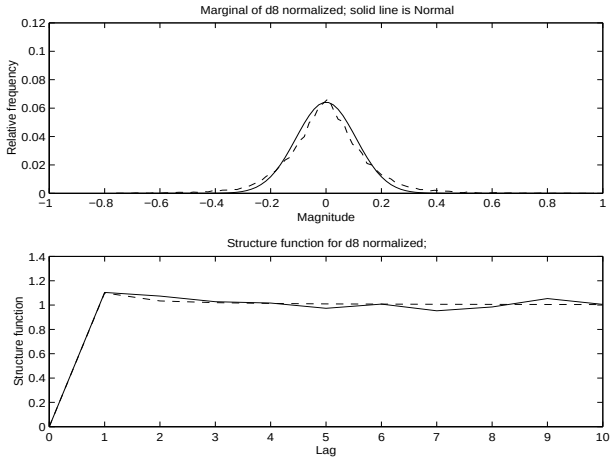

FIGURE 3. The top plot shows the empirical distribution of d_8. The solid line is a Gaussian distribution. The bottom plot shows the variogram of these wavelet coefficients. The dashed line is the theoretical variogram for fBm with $H = 1/3$.

FIGURE 4 (figstatint.ps)

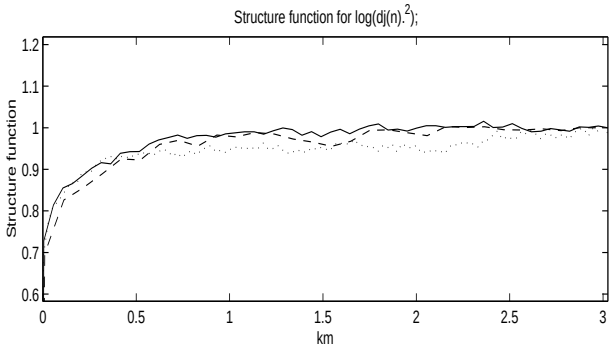

FIGURE 4. The figure shows the variogram of $\log(d_j(n)^2)$ as function of spatial lag and with $7 \leq j \leq 9$. The magnitude of these quantities determine the scale spectrum and they decorrelate over a scale on the order of km. The dotted, dashed and solid lines corresponds respectively to scales 7,8 and 9.

FIGURE 5 (FigPlotScaleSpect.ps)

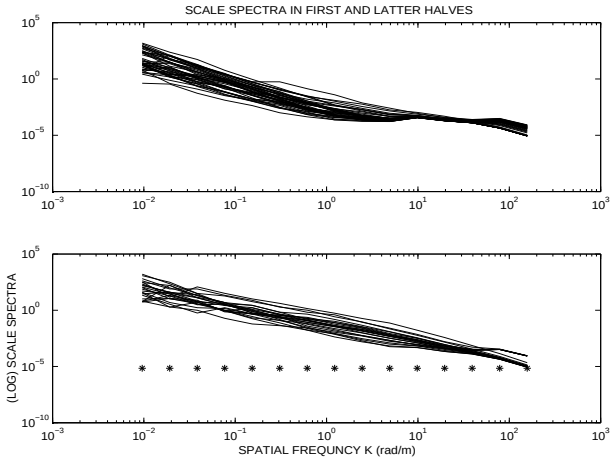

FIGURE 5. Scale spectra of nonoverlapping segments of the data (2^{15} points per segment) obtained from the Haar wavelet decomposition. The top plot corresponds to the first half of the data whereas the bottom plot corresponds to the second half. The scale spectra are plotted in log-log format. A line with slope -5/3 as in Kolmogorov spectra is also shown. The stars in the bottom plot corresponds to the different scales.

FIGURE 6 (FigPlotlevel.ps)

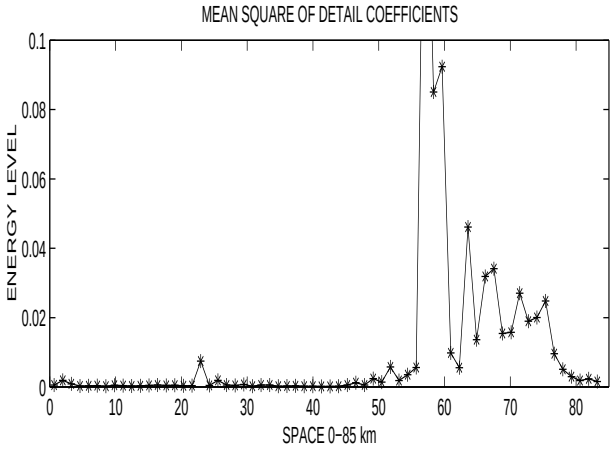

FIGURE 6. The figure shows the mean square of the d_8 wavelet coefficients when the data vector has been segmented into spatial segments of length $655m$. Note that the section in between $50km$ and $85km$ corresponds to a strong turbulence regime.

FIGURE 7 (FigPlotaeros.ps)

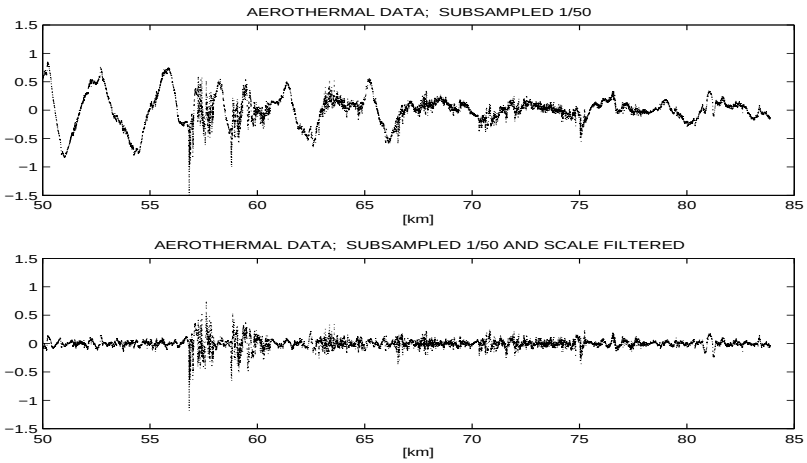

FIGURE 7. The top plot shows the strong turbulence section of the atmospheric temperature data. The bottom plot shows the atmospheric temperature data after it has been high-pass filtered using $db15$ wavelets.

FIGURE 8 (FigPlotinertial.ps)

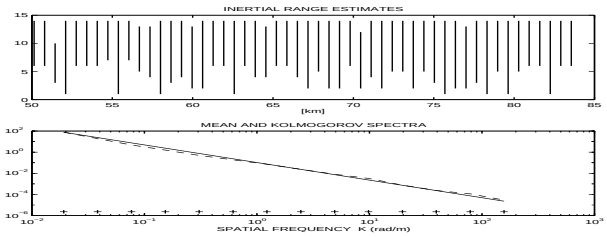

FIGURE 8. The vertical lines in the top plot are the estimates of the location dependent inertial ranges. That is, the scales over which the observed process is approximately a power law. For each segment of length 2^{15} points there is one vertical line showing the scales included in the inertial range estimate. In the bottom plot we show the average of the spectra. Note the excellent match with the Kolmogorov scaling law shown by the solid line!

FIGURE 9 (FigPlotPar.ps)

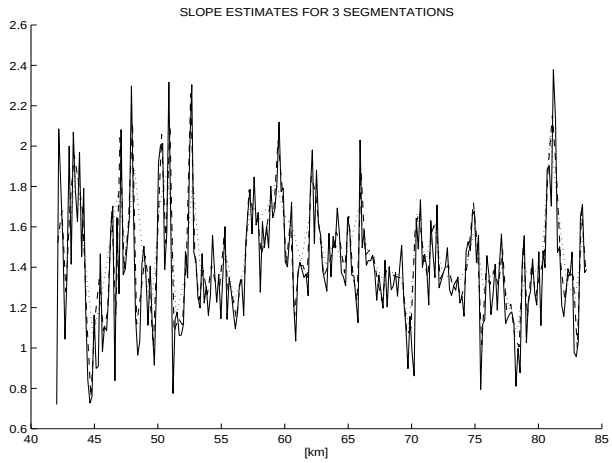

FIGURE 9. The figure shows slopes of log-log scale spectra from wavelet decompositions based on three different segment lengths. At the finest resolution the scale spectra are calculated over nonoverlapping segments 160m long. This is the solid line that has the largest variations. At the next resolution the nonoverlapping segments are 327m long (plotted with a dashed line). The coarsest resolutions is 655m and is shown with dotted line.

FIGURE 10 (FigPlotvariop.ps)

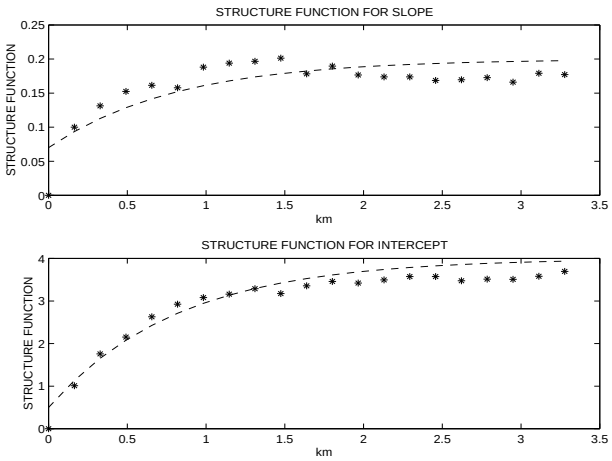

FIGURE 10. Variograms for the fluctuations of the slope (top) and log intercept (bottom) processes obtained from the temperature data. The stars are the variograms. The solid lines are fitted exponentials. We use slope and log intercept estimates from the data with the finest, $160m$, resolution.

FIGURE 11 (FigPlotFiltp.ps)

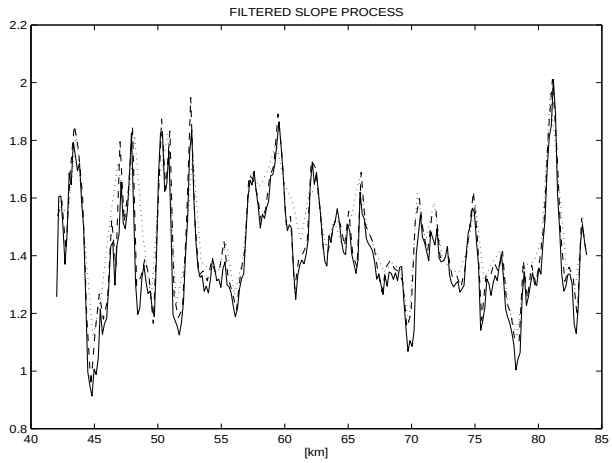

FIGURE 11. Filtered slope process of the actual data for the three finest segmentations. Note that the filtered processes for all three segmentations are essentially the same. The solid line corresponds to the finest resolutions. The dashed and dotted curves correspond to the two coarsest segmentations. The filtering has eliminated the differences in the slope processes that are due to the segmentation (as in Figure 9) by removing the white noise component of the slope fluctuations that is due to sampling.

FIGURE 12 (FigPlotFilti.ps)

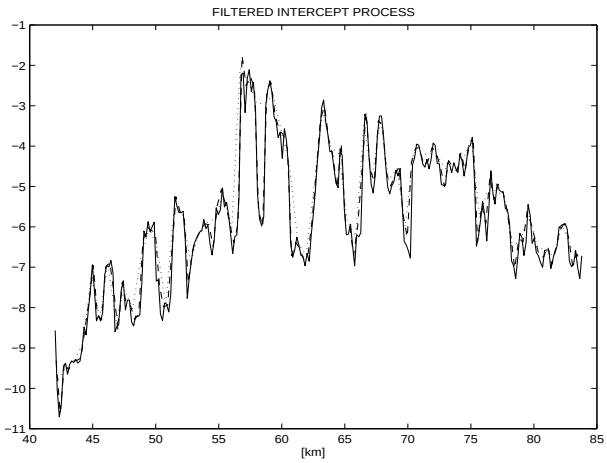

FIGURE 12. Filtered intercept process of the actual data for the three finest segmentations. The solid line corresponds to the finest resolutions, the dashed and dotted curves correspond to the two coarsest segmentations.

FIGURE 13 (FigPlotScfilt.ps)

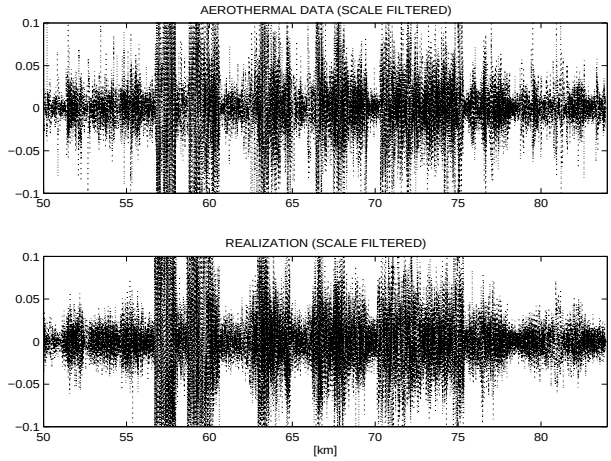

FIGURE 13. The *actual* temperature data set (top figure) obtained by synthesizing it from the detail coefficients in the range 6 to 11 of its Haar decomposition, corresponding to spatial scales of about 1 to 40 meters. Information from this range of scales enters into the estimates of the slope and log intercept processes. The bottom figure is the same as the top but for the *simulated* data. Note the striking similarity between the two figures.

FIGURE 14 (figgfunc.ps)

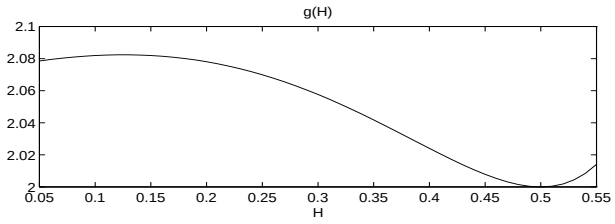

FIGURE 14. Plot of $g(H)$ showing how the relative variance of the scale spectrum depends on H.

FIGURE 15 (figdistr.ps)

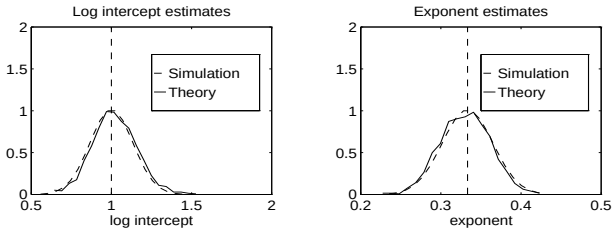

FIGURE 15. Distribution of power law parameter estimates. The parameters were estimated based on realizations of length 2^{10} with $H = 1/3$ and $\sigma^2 = 2$. The power law fitting is done over scales $1 \cdots 5$. The solid line is the empirical distribution associated with 1000 realizations, the dashed line is the theoretical distribution and the vertical lines are the specified parameters.

FIGURE 16 (figprec.ps)

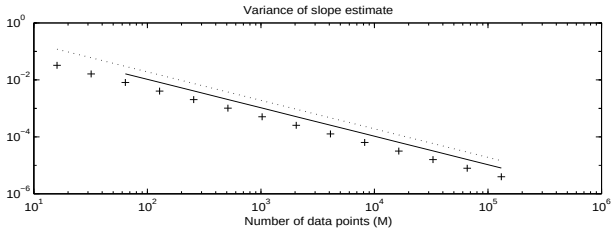

FIGURE 16. The variance of the slope estimate, computed by (6.22) with $H = 1/3$, is plotted as a function of the number of data points 2^M. The dotted line is for an estimate with three scales, the solid line with five scales. The crosses correspond to the Cramer-Rao lower bound. Note that even when the number of data points is not very large the estimate of the slope does not depend sensitively on the number of scales used.